Solar Physics
DOI: 10.1007/•••••-•••-•••-••••-•

Polarization calibration of the *Chromospheric Lyman-Alpha SpectroPolarimeter* for a 0.1% polarization sensitivity in the VUV range. Part II : In-flight calibration.

G. Giono[1] · R. Ishikawa[1] · N. Narukage[1] · R. Kano[1] · Y. Katsukawa[1] · M. Kubo[1] · S. Ishikawa[2] · T. Bando[1] · H. Hara[1] · Y. Suematsu[1] · A. Winebarger[3] · K. Kobayashi[3] · F. Auchère[4] · J. Trujillo Bueno[5] · S. Tsuneta[2] · T. Shimizu[2] · T. Sakao[2] · J. Cirtain[3] · P. Champey[6] · A. Asensio Ramos[5] · J. Štěpán[7] · L. Belluzzi[8,9] · R. Manso Sainz[10] · B. De Pontieu[11] · K. Ichimoto[12] · M. Carlsson[13] · R. Casini[14] · M. Goto[15]

Abstract The *Chromospheric Lyman-Alpha SpectroPolarimeter* is a sounding rocket instrument designed to measure for the first time the linear polarization of the hydrogen Lyman-α line (121.6 nm). The instrument was successfully launched on September 3, 2015 and observations were conducted at the solar

[1] National Astronomical Observatory of Japan, National Institutes of Natural Sciences email: gabriel.giono@nao.ac.jp
[2] Institute of Space and Astronautical Science, Japan Aerospace Exploration Agency
[3] NASA Marshall Space Flight Center
[4] Institut d'Astrophysique Spatiale, CNRS/Université Paris-Sud 11
[5] Instituto de Astrofísica de Canarias
[6] University of Alabama in Huntsville
[7] Astronomical Institute, Academy of Sciences of the Czech Republic
[8] Istituto Ricerche Solari Locarno
[9] Kiepenheuer-Institut für Sonnenphysik
[10] Max-Planck-Institut für Sonnensystemforschung
[11] Lockheed Martin Solar and Astrophysics Laboratory
[12] Hida Observatory, Kyoto University
[13] University of Oslo
[14] High Altitude Observatory, National Center for Atmospheric Research
[15] National Institute for Fusion Science, National Institutes of Natural Sciences

disc center and close to the limb during the 5-minutes flight. In this paper, the disc center observations are used to provide an in-flight calibration of the instrument's spurious polarization. The derived in-flight spurious polarization is consistent with the spurious polarization levels determined during the pre-flight calibration and a statistical analysis of the polarization fluctuations from solar origin is conducted to ensure a 0.014% precision on the spurious polarization. The combination of the pre-flight and the in-flight polarization calibrations provides a complete picture of the instrument's response matrix, and a proper error transfer method is used to confirm the achieved polarization accuracy. As a result, the unprecedented 0.1% polarization accuracy of the instrument in the vacuum ultraviolet is ensured by the polarization calibration.

Keywords: Polarization calibration, Vacuum UltraViolet, Lyman-alpha, Solar chromosphere, CLASP

1. Introduction

The *Chromospheric Lyman-Alpha SpectroPolarimeter* (CLASP) is a sounding rocket instrument designed to observe the linear polarization of the Lyman-α (121.56 nm) line with high spectral resolution and polarimetric sensitivity (Kano et al., 2012; Kobayashi et al., 2012). The core of this spectral line is emitted at the base of the solar transition region, while the wings of the line form more deeply in the upper-chromosphere. The high intensity of the Lyman-α radiation is particularly useful for studying the polarization emitted in this region, where the temperature rapidly rises from the chromospheric 10^4K to more than 10^6K in the corona.

In addition, although the contribution of the Zeeman effect to the polarization of the Lyman-α radiation is expected to be negligible, anisotropic radiation pumping processes in the upper chromosphere can produce measurable linear scattering polarization signals in the core and wings of the line (Trujillo Bueno et al., 2011; Belluzzi et al., 2012; Štěpán et al., 2012). The line-core ($\pm$0.2 nm around the line-center) polarization signal is also expected to be sensitive to the Hanle effect (*i.e.* the magnetic-field-induced modifications of the scattering line polarization; Hanle, 1924; Landi Degl'Innocenti and Landolfi, 2004), opening up a new diagnostic tool for studying the magnetic field of the upper solar chromosphere and transition region (Trujillo Bueno, 2014). Due to the small level of polarization signals from the scattering and the small polarization changes expected from the Hanle effect, an unprecedented polarization accuracy (<0.1%) in the Lyman-α line-core was required for the CLASP instrument.

A unique pre-flight polarization calibration experiment was conducted at Lyman-α under vacuum condition (Giono et al., 2016a), which determined the instrument's response matrices $\mathbf{X}$ (Elmore, 1990) for each of the two channels inside the spectro-polarimeter (design presented in Narukage et al., 2015). This response matrix is defined as $\mathbf{S'}=\mathbf{XS}$, where $\mathbf{S}$ is the incoming polarization signal expressed with its Stokes vector as $(I,Q,U)^\top$ and $\mathbf{S'}$ the measured polarization signal: $(I',Q',U')^\top$. Note that Stokes V was not considered for CLASP since the

instrument is designed for measuring only the linear polarization, which therefore reduces the $\mathbf{X}$ matrix to a 3×3 matrix. Cross-talks from Stokes V to Q' and U' were verified to be negligible in Giono et al. (2016a). The response matrix is composed of the spurious polarization (x_{01} and x_{02}), the spurious intensity (x_{10} and x_{20}), the scale factor (x_{11} and x_{22}) and the azimuth error (x_{21} and x_{12}) terms. The tolerance on these terms was derived by Ishikawa et al. (2014) and is recalled in Table 1. As discussed in Ishikawa et al. (2014) and based on these requirements, the 0.1% polarization accuracy of the instrument can be met at 2-σ level after combining all the errors.

Table 1. Tolerance for the response matrix elements, as taken from Ishikawa et al. (2014).

	Spurious polarization (x_{01} and x_{02})	Scale factor (x_{11} and x_{22})	Azimuth error (x_{21} and x_{12})
Requirement	0.017%	2%	0.5°
Tolerance ($\pm\sigma$)	1.7×10^{-4}	2.0×10^{-2}	1.7×10^{-2}

For convenience, the response matrices derived in Giono et al. (2016a) are recalled in Equation (1), with X_1 referring to channel 1's response matrix and X_2 referring to channel 2's response matrix.

$$\begin{aligned} X_1 &= \begin{pmatrix} x_{00} & x_{10} & x_{20} \\ x_{01} & x_{11} & x_{21} \\ x_{02} & x_{12} & x_{22} \end{pmatrix} = \begin{pmatrix} 1 & -0.0020 & 0.0004 \\ 0.00015 & 0.9765 & 0.0089 \\ 0.00002 & -0.0088 & 0.9763 \end{pmatrix} \\ X_2 &= \begin{pmatrix} x_{00} & x_{10} & x_{20} \\ x_{01} & x_{11} & x_{21} \\ x_{02} & x_{12} & x_{22} \end{pmatrix} = \begin{pmatrix} 1 & 0.0023 & -0.0004 \\ 0.00011 & 0.9708 & 0.0054 \\ 0.00005 & -0.0052 & 0.9706 \end{pmatrix} \end{aligned} \tag{1}$$

The 1σ error on each matrix element was estimated during the experiment and is expressed by $\Delta\mathbf{X}$, as recalled in Equation (2). These errors can be compared to their corresponding required tolerances from Table 1.

$$\begin{aligned} \Delta X_1 &= \pm \begin{pmatrix} \sigma_{00} & \sigma_{10} & \sigma_{20} \\ \sigma_{01} & \sigma_{11} & \sigma_{21} \\ \sigma_{02} & \sigma_{12} & \sigma_{22} \end{pmatrix} = \pm \begin{pmatrix} 0 & 0.0002 & 0.0005 \\ 0.00034 & 0.0020 & 0.0040 \\ 0.00039 & 0.0037 & 0.0020 \end{pmatrix} \\ \Delta X_2 &= \pm \begin{pmatrix} \sigma_{00} & \sigma_{10} & \sigma_{20} \\ \sigma_{01} & \sigma_{11} & \sigma_{21} \\ \sigma_{02} & \sigma_{12} & \sigma_{22} \end{pmatrix} = \pm \begin{pmatrix} 0 & 0.0005 & 0.0005 \\ 0.00039 & 0.0019 & 0.0052 \\ 0.00053 & 0.0045 & 0.0019 \end{pmatrix} \end{aligned} \tag{2}$$

All the matrix elements were properly determined within their respective tolerances by the pre-flight calibration except for the spurious polarization terms, for which the achieved ∼0.04% accuracy was larger than the 0.017% requirement. Achieving the tight accuracy required on the spurious polarization terms was

hard due to cross-talks from the linear polarization to the intensity (*i.e.* the x_{10} and x_{20} terms). These cross-talks were non-negligible during the pre-flight calibration as the Lyman-α light-source provided a fully-linearly-polarized input. The resulting effect of these cross-talks on the measured polarization was similar to the spurious polarization, and therefore limited the achieved accuracy on the spurious polarization terms.

The polarization coordinate system for the Stokes parameters used to describe the polarization states is defined as shown in Figure 1 (similar to Giono et al., 2016a; Ishikawa et al., 2014). The $+Q$ direction is defined along the spectrograph slit (X-axis), and the other Stokes directions ($+U$, $-Q$ and $-U$) are defined as clockwise as seen from the entrance aperture of the telescope. This definition is used for the calibration of the instrument.

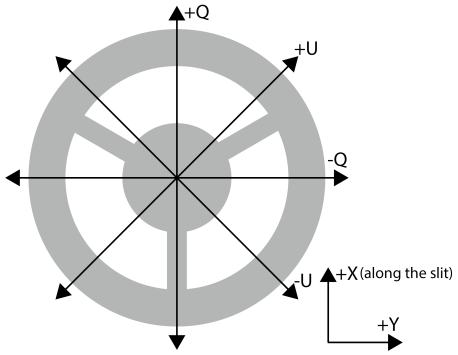

Figure 1. CLASP polarization coordinate system as seen from the entrance aperture of the instrument. The telescope's entrance aperture is shown in grey in the background.

The CLASP instrument was successfully launched on September 3, 2015 on-board a BlackBrand IX sounding rocket from the White Sands Missile Range (New Mexico, USA). Observations were conducted at the solar disc center for around 20 seconds, before re-pointing close to the limbs (*i.e.* main science target) for about 280 seconds (Kano et al., 2016). The disc center was observed to provide an in-flight calibration of the spurious polarization: the atomic-level polarization was expected to vanish at μ=1 (*i.e.* μ is the cosine of the heliocentric angle between the line-of-sight and the surface normal) due to symmetry in the plane parallel atmosphere. Although more realistic three-dimensional calculations suggested that the local anisotropy of the radiation field due to the chromospheric temperature and density topology variations can also create scattering polarization locally even at the solar disc center (Štěpán et al., 2015), the cancellation of the atomic-level polarization and the Hanle effect is still expected by spatially averaging the polarization signals measured along the slit at the disc center. By doing so, the spurious polarization level of the instrument can be estimated from the disc center measurements for both the channels.

The results from the in-flight polarization calibration on the spurious polarization levels of the instrument are presented hereafter and compared to the pre-flight calibration results recalled in Equation (1). A proper error transfer method from the response matrix to the corrected polarization signal is also

discussed and tested to ensure the polarization accuracy after corrections, before concluding on the instrument's response matrix and achieved polarization accuracy.

2. In-flight polarization calibration

Typical exposures observed at the disc center by the slit-jaw and the spectro-polarimeter are shown in Figure 2.

The 400"-length and 1.45"-width slit can be seen at the center of the slit-jaw image. The plate scales are 1.03" (slit-jaw spatial), 1.11" (spectro-polarimeter spatial) and 0.0048 nm (spectro-polarimeter spectral) on the 13 µm pixel CCD cameras (Narukage et al., 2015). From the optical alignment of the instrument, a ∼3" spatial resolution is expected on both the slit-jaw and the spectro-polarimeter. The spectro-polarimeter's spectral resolution is around 0.010 nm for both the channels. The achieved performances of the instrument were verified using the flight observations, which confirmed these spatial and spectral resolutions (Giono et al., 2016b).

The slit-jaw images were co-aligned with full-disc images 30.4 nm band from the *Atmospheric Imaging Assembly* (AIA onboard the *Solar Dynamics Observatory* spacecraft; Lemen et al., 2012) to determine the location of center of the slit in the solar coordinate reference: $(-16.3'', -12.1'')$, with (X,Y) where the positive X-axis is toward the solar-west and the positive Y-axis toward the solar-north. The center-to-limb variation of the Q/I line-center polarization signals, calculated assuming complete frequency redistribution in the one-dimensional (1D) quiet Sun model atmosphere of Fontenla et al. (1993), can be seen in the left panel of Figure 2 from Trujillo Bueno et al. (2011), with calculated line-center Q/I amplitude equal to 0.1% at $\mu = 0.9$ and exactly zero at $\mu = 1$. The errors in the scattering polarization due to the deviation from the actual Sun-center in the case of the CLASP observations at disc center were confirmed to be negligible by comparing with calculations of the scattering polarization along the slit. These calculations were carried out by means of the analytical solution of the scattering polarization in the Lyman-α line based on the two level atomic model and the anisotropic radiation field in the 1D quiet Sun atmosphere of Fontenla et al. (1993) (Goto et al., in prep.; Ishikawa et al., in prep.).

Although observations at the disc center were conducted during about 20 seconds, jitter of the rocket degraded the quality of the first exposures. Only three rotations of polarization modulation unit (PMU ; Ishikawa et al., 2015), which continuously rotates the half-waveplate and generates an exposure signal every 0.3 sec (every 22.5°, full rotation: 4.8 s) were selected for the analysis after stabilization of the pointing, corresponding to 48 images (taken in 14.4 s total). The demodulation was carried out after subtraction of the dark current (*i.e.* dark images were taken with the door closed, before and after the observation) and correction of the gain (*i.e.* gain of 2 for both the CCDs) using the scheme introduced in Equation (3), where D_i is the measured intensity taken at the i^{th} exposure for a given PMU rotation. Since three PMU rotations were stacked, the demodulated Q'/I' was calculated by using all 48 images from i=1 to i=48,

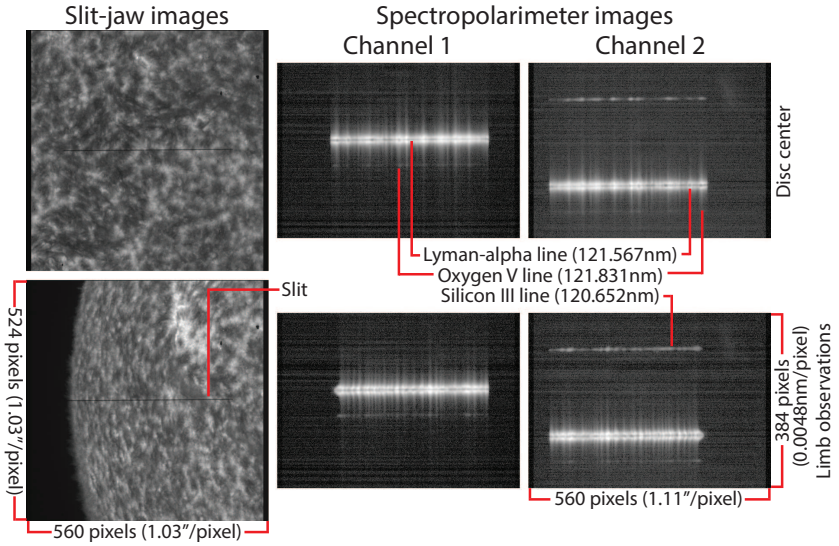

Figure 2. Typical raw exposures recorded at disc center for the slit-jaw (left) and the spectro-polarimeter (middle and right). Intensity is displayed in logarithmic scale. Channel 2's spatial direction is flipped compared to channel 1 due to the polarization analyzer's different orientation.

as in: $D_1-D_2-D_3+D_4+D_5-D_6-...-D_{47}+D_{48}$ for the numerator in Equation (3), and similarly for U'/I' but starting from i=2 to i=49 instead. This demodulation scheme is valid only for channel 2: a minus sign has to be applied when demodulating channel 1 due to the different orientation of the polarization analyzers.

$$\begin{aligned}\frac{Q'}{I'} &= \frac{\pi}{2}\left(\frac{D_1 - D_2 - D_3 + D_4 + D_5 - D_6 - D_7 + D_8 + ...}{D_1 + D_2 + D_3 + D_4 + D_5 + D_6 + D_7 + D_8 + ...}\right)\\ \frac{U'}{I'} &= \frac{\pi}{2}\left(\frac{D_2 - D_3 - D_4 + D_5 + D_6 - D_7 - D_8 + D_9 + ...}{D_2 + D_3 + D_4 + D_5 + D_6 + D_7 + D_8 + D_9 + ...}\right)\end{aligned} \tag{3}$$

Note that this demodulation scheme for U'/I' is slightly different from the one used in Giono et al. (2016a), and minimizes the possible spurious polarization error on U'/I' caused by the $\mathrm{d}I/\mathrm{dt}$ if the intensity of the observed source fluctuates during the modulation (see Appendix D). This effect was observed to be significant for the flight data when using the demodulation scheme from Giono et al. (2016a).

Figure 3 shows the demodulated Stokes parameters I', Q'/I' and U'/I' of the Lyman-α line along the slit and around the Lyman-α line for both the channels.

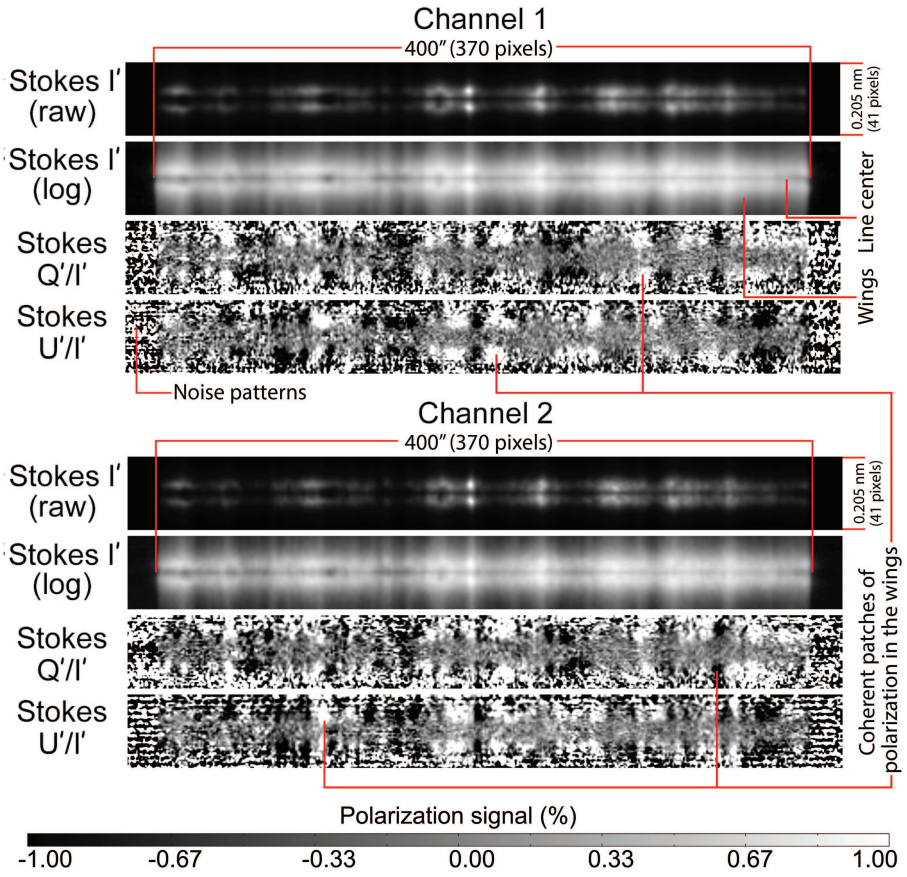

Figure 3. Demodulated Stokes parameters I', Q' and U' along the slit and around the Lyman-α line-core for both the channels. Any polarization signals larger than $+1\%$ and smaller than -1% is displayed as $+1\%$ and -1%, respectively.

Coherent patches of polarization can be seen in the wing parts of the Lyman-α line, as indicated in Figure 3. The amplitude of the polarization signal in these patches is clearly different from the noise and/or from a random pattern, indicating that the scattering polarization does not completely vanish even at disc center. The local anisotropy of the radiation field is a possible explanation for these scattering polarization patches. Although this effect is clearly stronger in the wing part of the line, it can also affect the line-core and spatial averaging along the slit was required to cancel this solar origin polarization. Figure 4 shows the integrated Stokes profiles for a full-slit summation, *i.e.* 360 pixels. The summation was performed on I', Q' and U' before dividing Q' and U' by I'. The measured Stokes Q'/I' and U'/I' at the line-core is within the range of the expected spurious polarization offset from Equation (1). The 1σ noise on the line-core polarization, composed of the photon noise, the read-out noise and the estimated error due to the residual polarization from the Sun (**i.e.** standard deviation of the polarization along the slit, divided by the square root of the number of pixels summed) can be seen to be comparable to the 1σ error on

the spurious polarization derived by the pre-flight calibration. The photon noise was calculated as the square root of the number of photoelectrons. The read-out noise was calculated based on the CCD calibration results of 6.2 and 6.5 e^- rms per pixel for channel 1 and channel 2, respectively (Champey et al., 2014, 2015). Variations of the signal larger than the noise can be seen in the wings, which indicate that the fluctuations from solar origin polarization might not be entirely cancelled out there. However, this is not a major issue for the in-flight calibration since stringent requirement on the spurious polarization is imposed only in the line core, as the Hanle effect only operates in this part of the line.

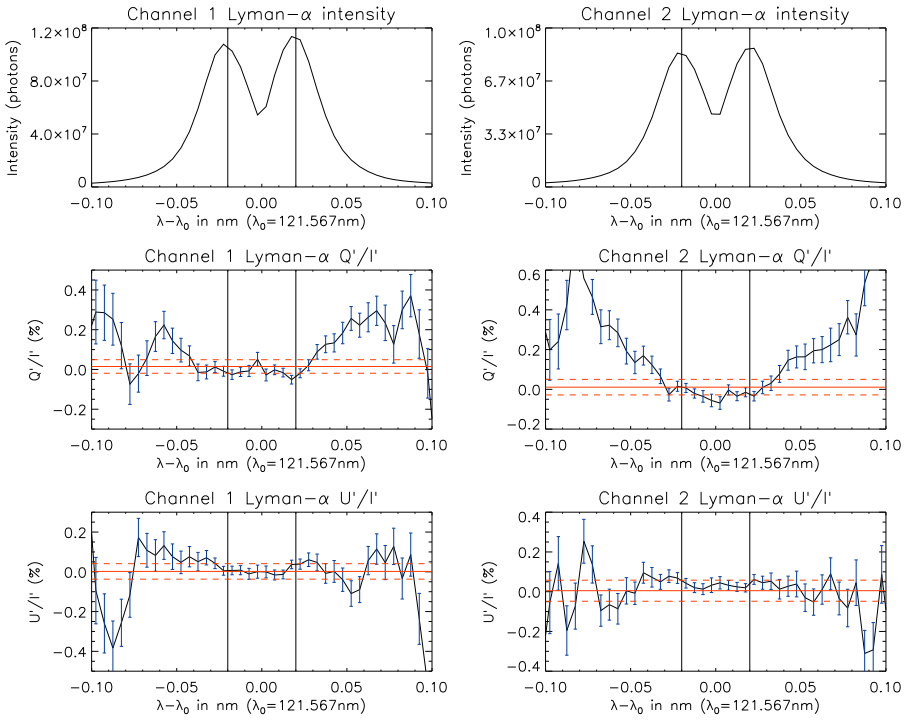

Figure 4. Stokes I', Q'/I' and U'/I' profiles obtained at disc center for a full slit spatially summed and three PMU rotations temporal summing, for both the channels. Horizontal red solid lines show the expected spurious polarization offsets from the pre-flight calibration, with dashed lines showing the $\pm 1\sigma$ error. Vertical black solid lines show the line-core (*i.e.* ± 0.02 nm around the line-center). Error bars shown in blue on the polarization signals indicate the noise (1σ), including the photon noise, the read-out noise and the error due to the residual polarization from the Sun for the full slit spatially summed.

The integrated polarization signal at the line-core and along the full slit can provide the spurious polarization level of the instrument with a better accuracy than previously derived during the pre-flight calibration. As previously mentioned, the limited accuracy achieved on the spurious polarization during the pre-flight experiment was caused by the contribution from the spurious intensity terms (*i.e.* x_{10} and x_{20}), substantial due to the fully-polarized light-source input (Giono et al., 2016a). However, this effect can be neglected in-flight, as the Sun's input is weakly polarized, and the spurious polarization levels can be

precisely determined as long as the residual polarization from solar origin can be cancelled out. For this purpose, a proper quantification of the error induced by this residual polarization, hereafter referred as solar fluctuations (*i.e.* as in fluctuations of the solar polarization along the slit), was required to ensure the accuracy of the spurious polarization. The analysis, explained in Appendix A, confirmed the normal distribution of the solar fluctuations, and its decrease with the square root of the number of pixel summed. Hence, the spurious polarization levels of the instrument were determined by integrating the full slit spatially and the line-core spectrally. The corresponding error was determined as the root sum square of the standard deviation of the solar fluctuations along the slit for the integrated line-core (σ=0.2%) divided by the square root of the number of pixels along the slit ($n_{\rm pixel}$=360), the photon noise and the read-out noise. Note that, considering the full slit and wavelength summation performed in this analysis, the resulting error from the combined photon noise and read-out noise was smaller by a factor of two compared to the error from the solar fluctuation. Results are summarized in Table 2 for both Q'/I' (*i.e.* x_{01}) and U'/I' (*i.e.* x_{02}), and both the channels. The error on the spurious polarization terms was derived with a better accuracy than the required 0.017% tolerance, meeting the requirement and also improving on while being consistent with the previous estimation from the pre-flight calibration. Note that the possible error from the non-uniformity of the PMU rotation discussed in Giono et al. (2016a) can be safely neglected here due to the very weak polarization measured.

Table 2. Final spurious polarization level for the flight, estimated as the full slit summation of the line-core. The 1σ error is determined as the root sum square of the standard deviation along the slit divided by the square root of the number of pixels, the corresponding photon noise and the corresponding read-out noise.

	Q'/I' (*i.e.* x_{01}, in %)	U'/I' (*i.e.* x_{02}, in %)
Channel 1	-0.015 ± 0.012	0.003 ± 0.014
Channel 2	-0.019 ± 0.012	0.033 ± 0.014

Figure 10 from Appendix A suggests that summing 120 pixels should be enough to reduce the polarization due to the solar fluctuation around the required accuracy. Hence, an estimation of the spurious polarization variation along the slit was attempted by summing the polarization signal every 120 pixels (*i.e.* 3 bins along the slit), and results are shown in Figure 5. The error bars show the solar fluctuations σ as determined with the standard deviation inside each bin. Variations larger than the 1σ error are observed and a non-linear trend along the slit can be seen in channel 1's Q'/I' and channel 2's U'/I'. No conclusive explanation were found for these different trends along the slit, and although the 120 pixels summing reduced the error to around 0.02%, residual polarization from the Sun might remain.

Nevertheless, the variation along the slit are still within 3σ accuracy and Figure 5 draws upper and lower boundaries for the possible variation of the spurious polarization along the slit, showing the variations along the slit to be within $\pm 0.07\%$ around the full-slit average spurious polarization. In addition, the pre-flight calibration presented in Giono et al. (2016a) also estimated the x_{01} and x_{02} terms along the slit (bottom, center and top), showing no particular trend within the $\sim 0.04\%$ accuracy achieved which is in-line with this result.

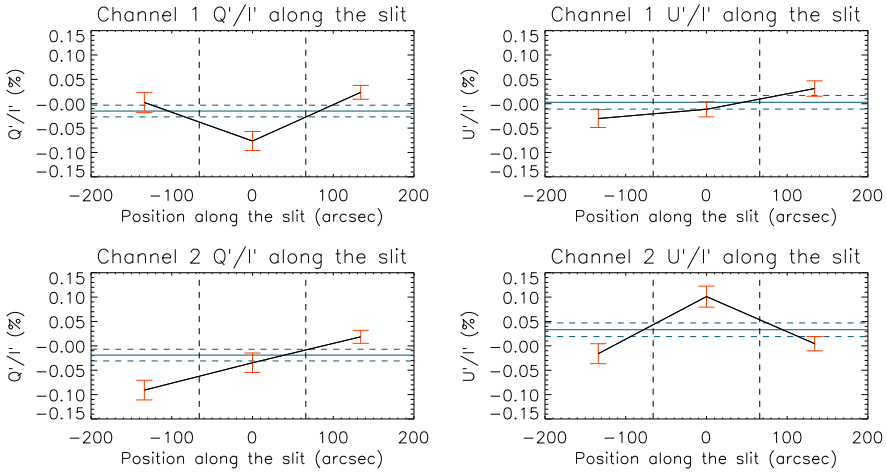

Figure 5. Q'/I' and U'/I' polarization signals along the slit, averaged every 120 pixels. The red error bars show the standard deviation of these values (1σ), calculated as the standard deviation on each 120-pixel regions. The horizontal blue solid line shows the spurious polarization derived for the full-slit summation in Table 2, with blue dash lines showing the $\pm 1\sigma$ error.

3. Correction of the polarization signal and error tranfer

The response matrix of the instrument $\mathbf{X}$ was finally determined within its required accuracy by combining the results from the pre-flight calibration with the spurious polarization terms obtained in-flight, as summarized in Equation (4) with updated values denoted in bold font. The corresponding $\pm 1\sigma$ error for each terms is also shown in Equation (4).

$$
\begin{aligned}
X_1 &= \begin{pmatrix} 1 & -0.0020 & 0.0004 \\ \mathbf{-0.00015} & 0.9765 & 0.0089 \\ \mathbf{0.00003} & -0.0088 & 0.9763 \end{pmatrix} \pm \begin{pmatrix} 0 & 0.0002 & 0.0005 \\ \mathbf{0.00012} & 0.0020 & 0.0040 \\ \mathbf{0.00014} & 0.0037 & 0.0020 \end{pmatrix} \\
X_2 &= \begin{pmatrix} 1 & 0.0023 & -0.0004 \\ \mathbf{-0.00019} & 0.9708 & 0.0054 \\ \mathbf{0.00033} & -0.0052 & 0.9706 \end{pmatrix} \pm \begin{pmatrix} 0 & 0.0005 & 0.0005 \\ \mathbf{0.00012} & 0.0019 & 0.0052 \\ \mathbf{0.00014} & 0.0045 & 0.0019 \end{pmatrix}
\end{aligned}
\tag{4}
$$

The response matrix elements can be used to correct the q' and u' polarization signals measured by the instrument in order to retrieve the q and u polarization

signals from the Sun. The equations linking these quantities were derived from $\mathbf{S'{=}XS}$ considering $S'{=}(1, Q'/I', U'/I')^\top{=}(1, q', u')^\top$ and $S{=}(1, q, u)^\top$ as:

$$
\begin{aligned}
q &= \frac{\left[(q' - x_{01}) - \frac{(u'-x_{02})(x_{20}q'-x_{21})}{(x_{20}u'-x_{22})}\right]}{\left[(x_{11} - x_{10}q') - \frac{(x_{10}u'-x_{12})(x_{20}q'-x_{21})}{(x_{20}u'-x_{22})}\right]} \\
u &= \frac{\left[(u' - x_{02}) - \frac{(q'-x_{01})(x_{10}u'-x_{12})}{(x_{10}q'-x_{11})}\right]}{\left[(x_{22} - x_{20}u') - \frac{(x_{20}q'-x_{21})(x_{10}u'-x_{12})}{(x_{10}q'-x_{11})}\right]}
\end{aligned}
\tag{5}
$$

The error on the corrected q and u was estimated taking into account the measurement error on the measured q' and u', as well as the error on each of the response matrix elements from Equation (4) using the error transfer formula shown in Equation (6) for q, and similarly for u.

$$
\sigma_q = \sqrt{\sum_i \left(\frac{\partial q}{\partial x_i}\sigma_i\right)^2} \quad \text{where } x_i = q', u', x_{10}... \text{ and } \sigma_i = \sigma_{q'}, \sigma_{u'}, \sigma_{x_{10}}... \tag{6}
$$

The partial derivatives of the two equations were calculated for all of the ten components. These partial derivatives express the importance (*i.e.* scaling factor) of the corresponding error depending on the polarization signal measured. The partial derivatives of the corresponding Stokes parameter (*e.g.* $\partial q/\partial q'$ for σ_q) and spurious polarization (*e.g.* $\partial q/\partial x_{01}$ for σ_q) are the most dominant factors when considering a weakly polarized input (*i.e.* <2%, as seen in the Lyman-α line-core), with values close to unity. Hence, the root sum square of the error on the Stokes parameters (*i.e.* photon noise and read-out noise) and the error on its corresponding spurious polarization matrix elements (*i.e.* x_{01} when correcting q' and x_{02} when correcting u') is a good approximation for determining the achieved accuracy in this case. However, for a larger polarization amplitude, the contributions from the partial derivatives of the spurious intensity, the scale factor, and the azimuth errors increase and the full partial derivatives formula should be used. An example for the partial derivatives for the observed q as a function of the measured q' and u' is shown in Appendix B.

For demonstrating the achieved accuracy after correction, the polarization signals were demodulated from the limb observations by stacking 50 PMU rotations (*i.e.* 240 s observation) and summing almost the entire slit (340 pixel) closer to the limb, from $\mu{\sim}0.02$ to $\mu{\sim}0.53$. The correction was applied on polarization signals using the equations previously described: Figure 6 shows the difference between the corrected and demodulated profiles for both the channels. The effect of the correction on the demodulated polarization signal is small because the response matrix of the instrument is close to the identity matrix: changes in the line-core are ∼0.02% and mainly due to the spurious polarization offset. On the other hand, the differences in the wings (*i.e.* region outside the line-core) are ∼0.1% for the Q/I signal due to the increase in polarization signal and the

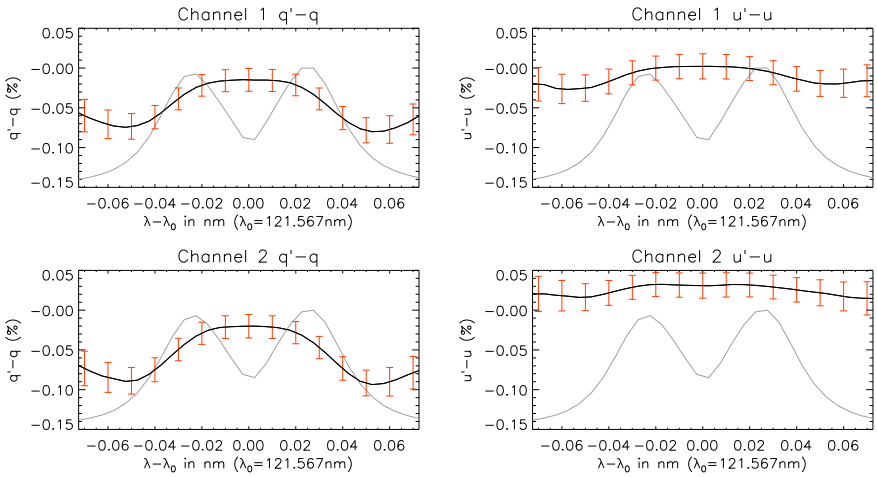

Figure 6. Residual between the corrected polarization (q' and u') and the observed polarization (q and u) for channel 1 (top row) and channel 2 (bottom row) as a function of wavelength. The corresponding intensity profile is shown in grey in the background to provide the location of the line-center, double peak and wings. Red error bars show the combined error on the corrected profiles (photon noise, read-out noise and response matrix error).

effect of the scale factor. Figure 7 shows the achieved accuracy on the corrected signal (*i.e.* error bars in Figure 6), using the error transfer method described previously to combine the various source of errors. The accuracy achieved is mainly influenced by the photon noise, as the wavelength dependence of the accuracy indicates, but also by the accuracy achieved on the spurious polarization terms. Note that performing spectral summing could improve the accuracy even further. Moreover, one can see that a better accuracy was achieved on Q/I compared to U/I: this is mainly due to the different accuracy achieved on the x_{01} and x_{02} terms in Table 2 (*i.e.* $\sigma_{x_{01}}$=0.012% and $\sigma_{x_{02}}$=0.014%). Other differences between the accuracy achieved on the two channels Q/I and U/I are due to a combination of the different scale factor and azimuth errors terms between $\mathbf{X}_1$ and $\mathbf{X}_2$ in Equation (4), as well as the difference in throughput between both the channels (*i.e.* different quantum efficiency of the CCDs, Champey et al. (2014)) affecting their respective photon noise.

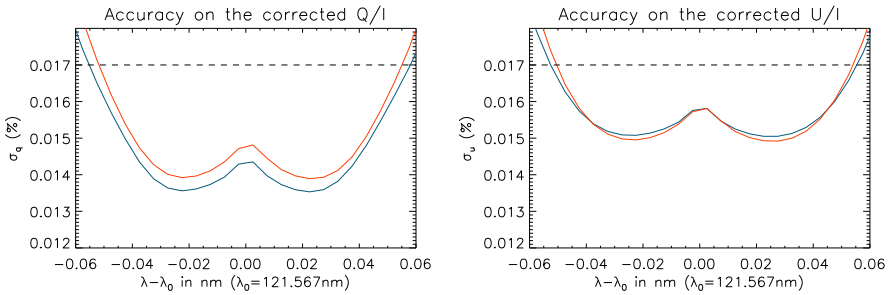

Figure 7. Accuracy achieved (1σ) on the corrected Q/I and U/I as a function of wavelength for channel 1 (blue curve) and channel 2 (red curve). The horizontal dashed line shows the 0.017% accuracy level.

The instrument accuracy can be discussed by comparing the polarization signals recorded in both the channels after correction: the profiles on both the channels overlap within a 2σ accuracy (σ=∼0.016%), which is smaller than our instrument requirement of 0.1% as shown in Figure 8. Note that a careful coalignment between the two channels was performed for the overlap, using interpolation to reach a subpixel precision. The difference between two channels is caused by the spurious polarization originating from the intensity fluctuation of the Sun, but also pointing jitter and drift, as the two channels simultaneously measure the two orthogonal polarization states. Therefore, combining the polarization signal from both the channels would improve the overall polarization accuracy achieved by the instrument even further.

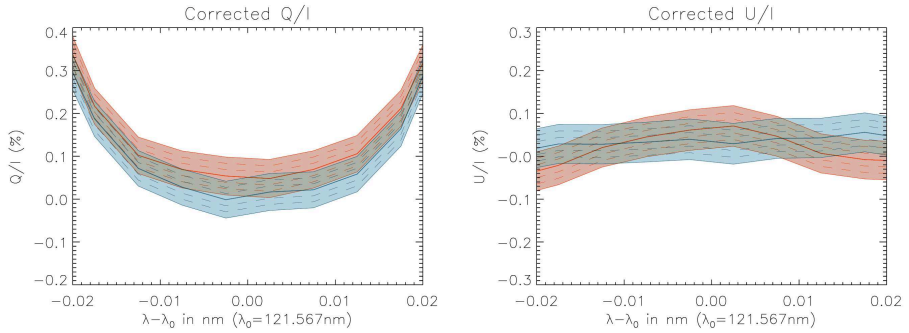

Figure 8. Comparison between corrected Q/I and U/I for channel 1 (blue) and channel 2 (red) at the line-core. The thick-line shows the recorded polarization signal, with dash-lines showing the 1σ, 2σ and 3σ contour, with σ taken from Figure 7.

It was observed that some differences remain between the two channels when using a smaller number of PMU rotations, and can sometimes be seen locally from pixel to pixel in the wavelength direction depending on the location along the slit selected for the spatial summation and/or number of PMU rotations stacked. Appendix C presents an example of such differences when using only 15 PMU rotations taken from the limb observations. These local differences are larger than the 3σ error derived and their origin is unclear. More detailed investigations were conducted to quantify the error induced by additional effects

not taken into account in the analysis, such as the drift of the slit observed on the CCD images over time (∼1 pixel in channel 1 and ∼2 pixels in channel 2 over the 5-minutes observation), the spurious polarization due to the dI/dt ($\sigma_{dI/dt}$=∼0.013% per PMU rotation and per pixel, estimated in Appendix D) or the jitter effects (σ_{jitter}=∼0.120% per PMU rotation and per pixel, estimated in Appendix E). Even so, none of these effects can clearly account for the local differences observed, as these errors are reduced by the square root of the number of PMU rotations stacked and pixel summed: the errors in the 15 PMU rotations example considered are $\sigma_{dI/dt}$<0.001% and σ_{jitter}∼0.002%, which is one order of magnitude smaller than the error derived in Figure 7. However, it is worth noticing that only a rough estimation for both the spurious polarization due to the dI/dt and due to the jitter effect was derived. Additionally, the possible variation of the intensity on time-scale shorter than the modulation time cannot be estimated and could also induce spurious polarization.

4. Conclusion

The response matrix of the instrument was initially determined from the pre-flight calibration (Giono et al., 2016a) but an uncertainty remained on the spurious polarization, determined with only a ∼0.04% accuracy. The flight observations carried out at the solar disc center were used to obtain a better estimation of the spurious polarization level and to better determine the response matrix. The x_{01} and x_{02} terms derived from this in-flight calibration were consistent with the values obtained during the pre-flight calibration, and were determined with a 0.014% accuracy, therefore fulfilling the 0.017% tolerance requirement. The response matrix was used to correct the demodulated polarization signal from the limb observations, using a proper transfer of the errors from the demodulated polarization and from the response matrix elements to conclude on the achieved accuracy. Comparison between the corrected Lyman-α line-core polarization from both the channels demonstrated a consistency at the 2-σ level with σ around 0.016%, indicating the 0.1% polarization accuracy of the CLASP instrument.

Appendix

A. Error induced by the solar origin polarization at disc center.

Figure 9 shows the histograms of the polarization signal along the slit for the integrated line-core (*i.e.* line-center ±0.02 nm). The standard deviation can be used to estimate the error σ caused by the solar fluctuations. This σ without pixel spatially summed (*i.e.* $\sigma_{\rm slit}$) is around 0.2% for both Q'/I' and U'/I', and for both the channels.

The solar fluctuations σ is expected to decrease as $1/\sqrt{n_{\rm pixel}}$, where $n_{\rm pixel}$ is the number of pixel spatially summed. However, this assumption is only true if the solar fluctuations are generated by a random process. The histogram shown in Figure 9 indicates that this assumption is reasonably true, as their shape is close to a normal distribution. Nevertheless, the variation of σ as a function of number of pixels for spatial summation was confirmed experimentally. Pixels were randomly selected along the slit and summed, and the process was repeated multiple time to artificially increases the limited number of sample available along the slit. The standard deviation was used to determine the solar fluctuations σ for each number of pixel summing. This method artificially increase the sample size, and is useful when the number of pixels summed is large. Results are shown in Figure 10, and confirmed the $\sigma_{\rm slit}/\sqrt{n_{\rm pixel}}$ decrease.

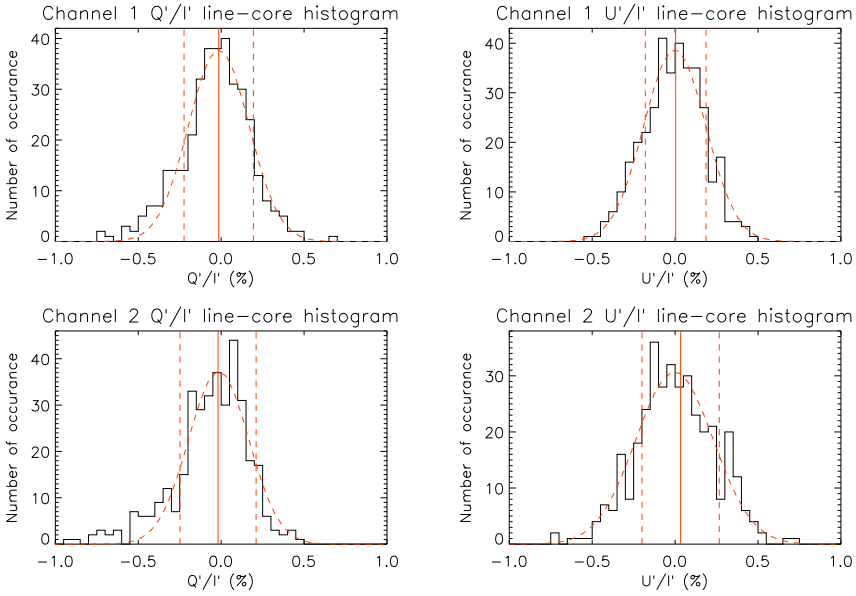

Figure 9. Histogram of the Q'/I' and U'/I' polarization signals along the slit for both the channels for the integrated line-core. Wavelength summing was performed at ±0.02 nm around the line-center. The $\pm\sigma$ from the standard deviation are shown by two vertical dashed red lines around the average value (vertical solid red).

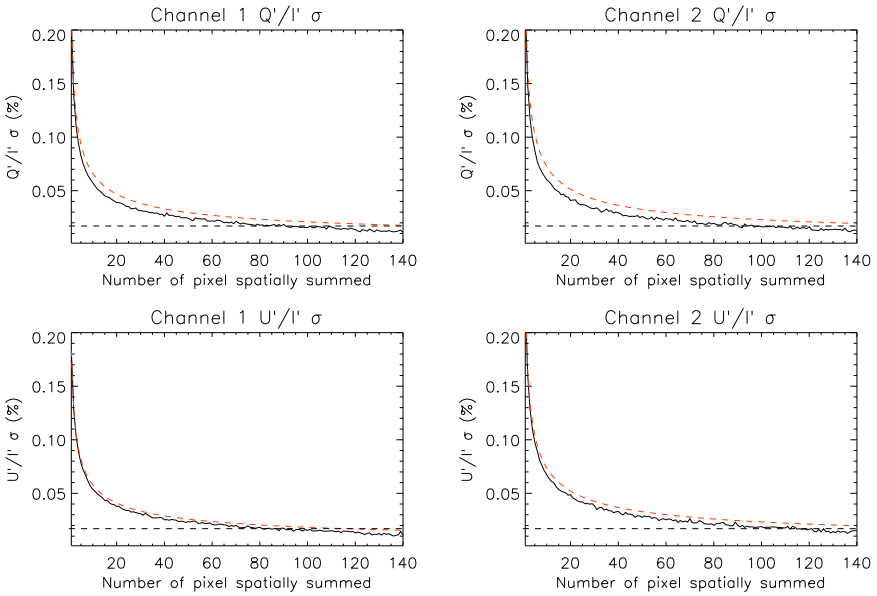

Figure 10. Evolution of the solar fluctuations σ as a function of the number of pixels summed spatially. The X-axis shows the number of pixels summed (n_{pixel}). Black solid lines show the σ calculated as the averaged σ_t (*i.e.* out of $N = 100$ values). For each n_{pixel}, the σ_t were obtained with the standard deviation of pixels randomly selected and summed along the slit. This process was repeated N times. The red dashed lines show the theoretical decrease of σ, taken as the σ for $n_{\mathrm{pixel}} = 1$ divided by $\sqrt{n_{\mathrm{pixel}}}$. Horizontal dashed lines show the 0.017% accuracy required on the spurious polarization.

B. Partial derivatives for error transfer

Figure 11 shows the partial derivatives of the q function for each of the ten components, as a function of the measured q' and u'. One can see that the $\partial q/\partial q'$ and $\partial q/\partial x_{01}$ derivatives are close to unity and almost insensitive to changes in q' and u'. On the other hand, the influence of the $\partial q/\partial x_{10}$ and $\partial q/\partial x_{11}$ derivatives increase with q'. It is also interesting to notice that the $\partial q/\partial u'$ term is proportional to its corresponding azimuth error term, and the contribution of $\partial q/\partial x_{22}$ scales with u'.

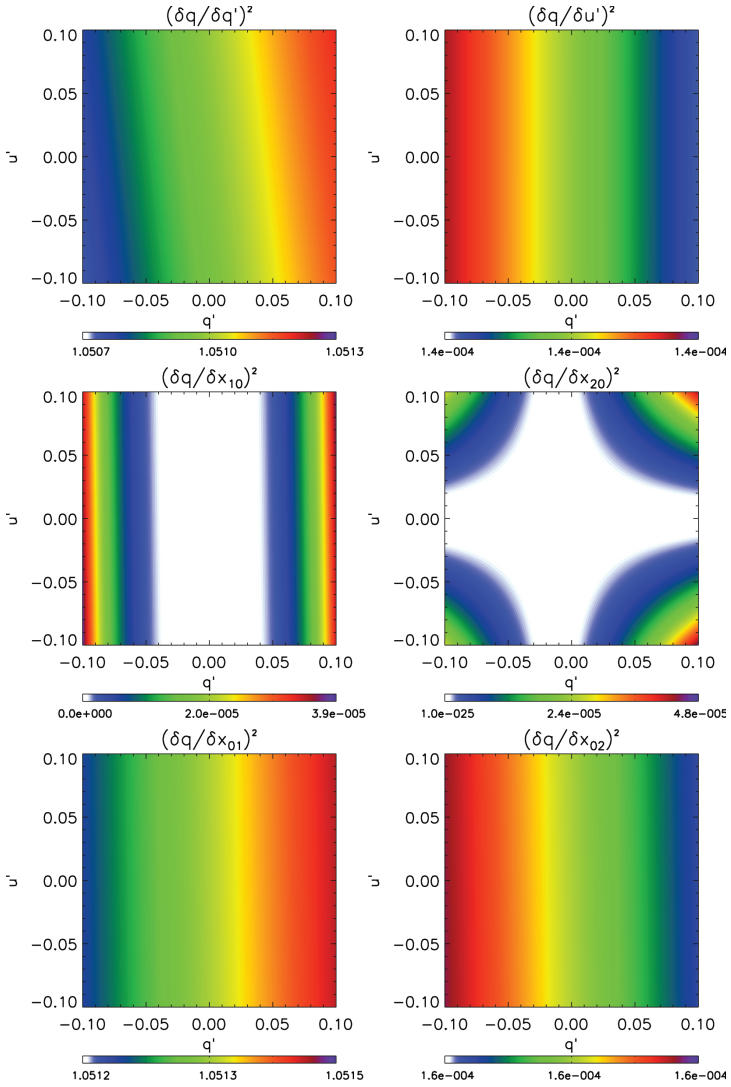

(a)

Figure 11. Partial derivatives squared of the q function with respect to the ten components, as a function of q' and u'.

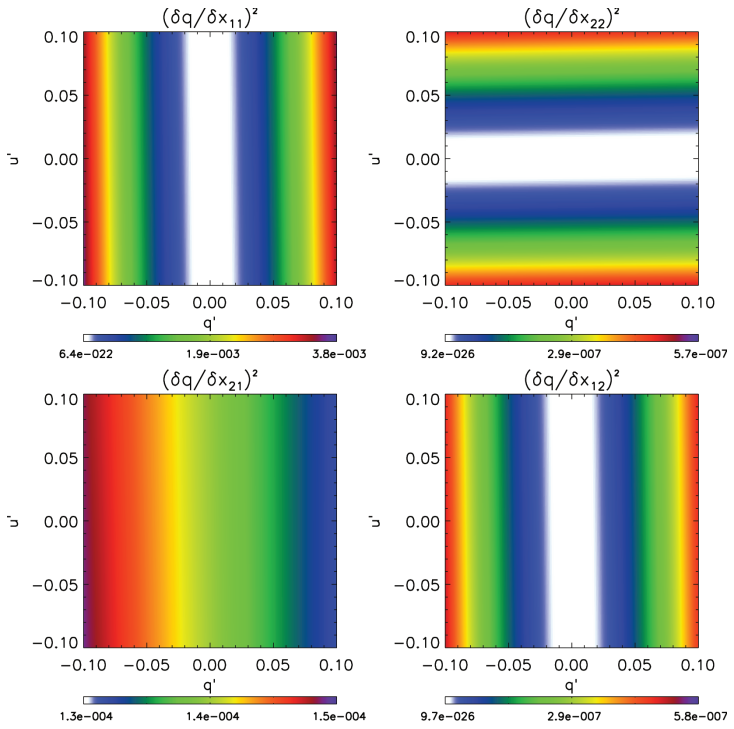

(b)

Figure 11. (continued)

C. Additional example: corrected signal using 15 PMU rotations

Figure 12 shows the corrected polarization profiles for both the channels when using only 15 PMU rotations from the limb observations. Although the achieved 1σ accuracy, shown in Figure 13, is below the required 0.017% level for Q/I, the profiles show a difference larger than 3σ at -0.002 nm. This difference is only seen locally and the profiles otherwise overlap within a 2σ accuracy. The origin for such difference is not precisely known but it indicates that additional errors might contribute when using a limited number of PMU rotations, such as error due to temporal variation of the intensity ($\mathrm{d}I/\mathrm{dt}$, see Appendix D), jitter error (see Appendix E) and pointing drift error.

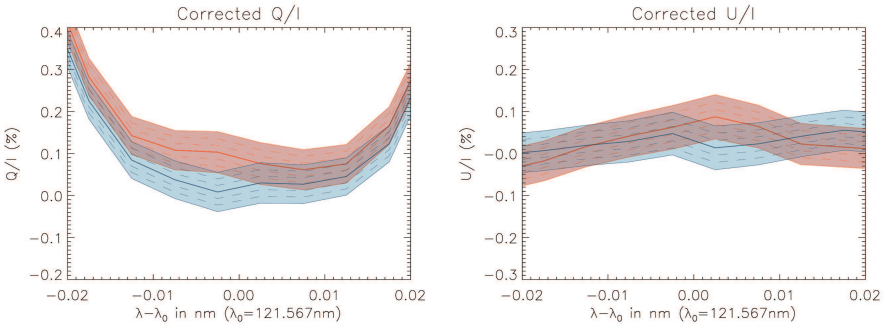

Figure 12. Comparison between corrected Q/I and U/I for channel 1 (blue) and channel 2 (red) at the line-core using only 15 PMU rotations taken from the observations at the limb. The thick-line shows the recorded polarization signal, with dash-lines showing the 1σ, 2σ and 3σ contour, with σ taken from Figure 13.

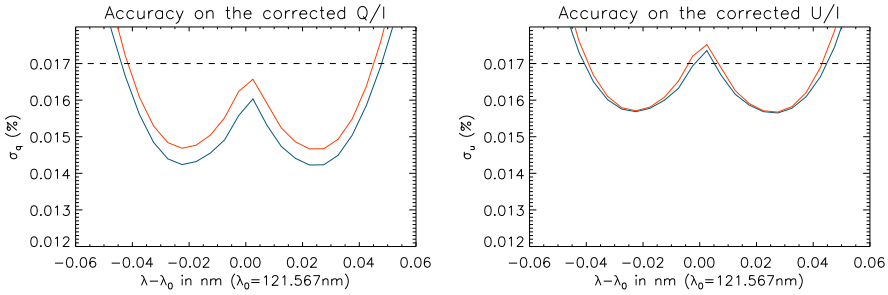

Figure 13. Accuracy achieved (1σ) on the corrected Q/I and U/I as a function of wavelength for channel 1 (blue curve) and channel 2 (red curve) for the profiles shown in Figure 12. The horizontal dashed line shows the 0.017% accuracy level.

D. Spurious polarization due to dI/dt

The spurious polarization due to the temporal variation of the intensity was estimated for each pixel following the method presented in Ishikawa et al. (2014). At first, the intensity variation per exposure and per pixel was estimated from the subtraction of two successive intensity images averaged over one complete PMU rotation (4.8s) using the formula $\Delta D = (D_i - D_{i+1})/(D_i + D_{i+1}) \times 0.3s/4.8s$, where D_i is the intensity image for the i^{th} PMU rotation from the observation at the limbs and the 0.3/4.8 factor is the scaling (*i.e.* linear interpolation) to one exposure. A histogram of the resulting intensity variation at each pixel per exposure and for each channel is shown in Figure 14. The standard deviation provides the σ_t of the intensity variation: 0.050% for channel 1 and 0.043% for channel 2. The spurious polarization from this dI/dt was then estimated using

Equation (7), where a is $2/\pi$ and c the number of exposure considered (see Appendix A.4.2 in Ishikawa et al., 2014).

$$\sigma_{dI/dt} = \frac{1}{a\sqrt{2c}}\sigma_t \tag{7}$$

Hence, the corresponding spurious polarization per complete PMU rotation (*i.e.* c=16) is 0.014% and 0.012% per pixel for channel 1 and channel 2, respectively. Note that, considering the number of PMU rotations and pixels summed at disc center (*i.e.* 3 PMU rotation, 360 pixels summed spatially and 9 pixels summed spectrally), the $\sigma_{dI/dt}$ for the disc center observation can be estimated around <0.001% for both the channels, which is negligible compared to the error derived on the spurious polarization in Table 2. It is also interesting to notice that the distribution of the intensity variation shown in Figure 14 peak around -0.1% for both the channels. This is due to the gradual throughput degradation observed during the flight. This degradation of the throughput was not a major issue because linear variation of the intensity does not induce spurious polarization, as it is cancelled by the demodulation scheme. Finally, it is also important to point out that the derived estimation for the dI/dt spurious polarization is quite rough, and it is impossible to estimate the spurious polarization caused by intensity disturbances which are not resolved spatially and/or temporally by the instrument. Hence, the observation might be affected even though the estimation for the dI/dt spurious polarization is very small.

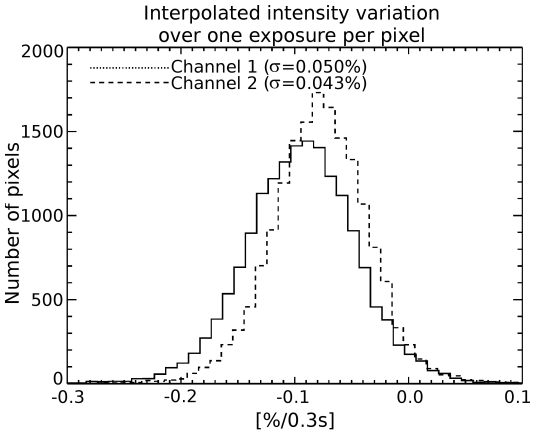

Figure 14. Histogram of the interpolated variation per exposure and per pixel.

E. Spurious polarization due to jitter

The spurious polarization caused by the pointing jitter was calculated by first interpolating the jitter profile obtained by analysing the slit-jaw images (see Figure 15, Kubo et al., 2016) taken at the limb with a 0.6 s cadence to the 0.3 s cadence of the spectro-polarimeter. The jitter shows a periodicity at 4.8 s,

mainly due to the image wobbling caused by the half-waveplate rotation. The intensity distribution along the slit was then obtained by temporally averaging the data from three PMU rotations and by averaging 6 pixels around the line-center. The temporal change of the intensity along the slit was simulated by combining the interpolated jitter information and the intensity distribution previously derived. Finally, the spurious polarization was derived from the estimated temporal change of the intensity, using the demodulation scheme. Figure 16 shows the estimated spurious polarization caused by the jitter when simulating for the entire observation at the limb. In this example, the σ_{jitter} is 0.009% for channel 1 and 0.010% for channel 2 for the full slit and 6 pixels summed in the wavelength direction. The σ_{jitter} per PMU rotation and per pixel can be estimated by multiplying these number by $\sqrt{53}\times\sqrt{6}$, resulting in 0.114% and 0.126% for channel 1 and channel 2, respectively.

Similarly as for $\sigma_{dI/dt}$ in Appendix D, the σ_{jitter} for the in-flight calibration at disc center can be estimated around 0.001% for both the channels (dividing it by $\sqrt{3}\times\sqrt{360}\times\sqrt{9}$), which is also negligible compared to the error derived on the spurious polarization in Table 2.

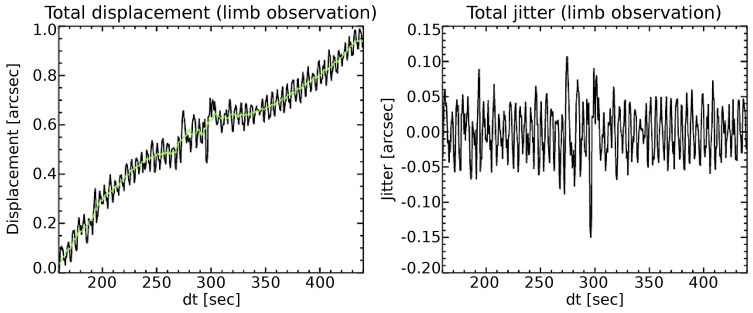

Figure 15. Total displacement (left) and total jitter (right, displacement removed) calculated from the slit-jaw observation at the limb. The total displacement (green line) is <0.9", and the jitter peak-to-valley is <±0.15".

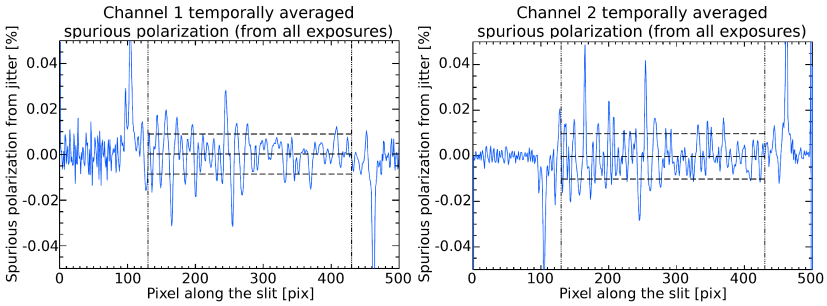

Figure 16. Temporally average (full observation at the limb, *i.e.* 53 PMU rotations and 6 pixels in wavelength summed) spurious polarization along the slit due jitter effect, for channel 1 (left) and channel 2 (right). The slit region is located between the two vertical dash lines.

Acknowledgments The authors acknowledge the *Chromospheric Lyman-Alpha Spectropolarimeter* (CLASP) team. The team was an international partnership between NASA Marshall Space Flight Center, National Astronomical Observatory of Japan (NAOJ), Japan Aerospace Exploration Agency (JAXA), Instituto de Astrofsica de Canarias (IAC) and Institut d'Astrop physique Spatiale; additional partners include Astronomical Institute ASCR, Lockheed Martin and University of Oslo. Japanese participation is funded by the basic research program of ISAS/JAXA, internal research funding of NAOJ, and JSPS KAKENHI Grant Numbers JP23340052, JP24740134, JP24340040, and JP25220703. US participation is funded by NASA Low Cost Access to Space (Award Number 12-SHP 12/2-0283). Spanish participation is funded by the Ministry of Economy and Competitiveness through project AYA2010-18029 (Solar Magnetism and Astrophysical Spectropolarimetry). French hardware participation was funded by Centre National d'Etudes Spatiales (CNES). J. Štěpán acknowledges the financial support by the Grant Agency of the Czech Republic through grant 16-16861S and project RVO:67985815.

References

Belluzzi, L., Trujillo Bueno J., Štěpán J., "The scattering polarization of the Ly-α Lines of H I and He II taking into account PRD and J-state interference effects", *Astrophys. J.*, 2012, 755:L2, DOI: 10.1088/2041-8205/755/1/L2

Champey P., Kobayashi K., Winebarger A., Cirtain J., Hyde D., Robertson B., Beabout D., Beabout B., Stewart M., "Performance characterization of UV science cameras developed for the Chromospheric Lyman-Alpha Spectro-Polarimeter (CLASP).", *Proc. of SPIE*, **9144**, 2014, DOI:10.1117/12.2057321

Champey P., Kobayashi K., Winebarger A., Cirtain J., Hyde D., Robertson B., Beabout B., Beabout D., Stewart M., "VUV testing of science cameras at MSFC: QE measurement of the CLASP flight cameras", *Proc. of SPIE*, **9601**, 2015, DOI: 10.1117/12.2188754

Elmore D.F., "A polarization calibration technique for the advanced stokes polarimeter.", *NCAR Technical Note*, 1990, NCAR/TN-355+STR, Boulder, Colorado, DOI:10.5065/D6959FHZ

Fontenla J. M., Avrett E. H., Loeser R., "Energy balance in the solar transition region. III - Helium emission in hydrostatic, constant-abundance models with diffusion.", *Astrophys. J.*, 1993, **406**, p.319-345, DOI:10.1086/172443

Giono G., Ishikawa R., Narukage N., Kano R., Katsukawa Y., Kubo M., Ishikawa S., Bando T., Hara H, Suematsu Y., Winebarger A., Kobayashi K., Auchère F. and Trujillo Bueno J., "Polarization calibration of the Chromospheric Lyman-Alpha SpectroPolarimeter for a 0.1% polarization sensitivity in the VUV range. Part I : Pre-flight calibration.", *Solar phys.*, 2015, DOI: 10.1007/s11207-016-0950-x

Giono G., Ishikawa R., Narukage N., Kano R., Katsukawa Y., Kubo M., Ishikawa S., Bando T., Hara H, Suematsu Y., Winebarger A., Kobayashi K., Auchère F. and Trujillo Bueno J., "Optical alignment of the Chromospheric Lyman-Alpha Spectro-Polarimeter using sophisticated methods to minimize activities under vacuum.", *Proc. of SPIE*, 2016, **9905**, DOI:10.1117/12.2232312

Hanle W., "Uber magnetische Beeinflussung der Polarisation der Resonanzfluoreszenz.", *Z. Phys*, 1924, 30:93

Goto M., Ishikawa R., Iida Y., Tsuneta S., "Analytical Solution of the Hanle effect in View of CLASP and Future Polarimetric Solar Studies" In preparation

Ishikawa R., Narukage N., Kubo M., Ishikawa S., Kano R., Tsuneta S., "Strategy for Realizing High-Precision VUV Spectro-Polarimeter", *Solar Phys.*, 2014, **289**, No.12, pp.4727, DOI:10.1007/s11207-008-9169-9

Ishikawa R., Uitenbroek H., Goto M., Iida Y., Tsuneta S., "Influence of the atmospheric model on the Hanle diagnostics", In preparation

Ishikawa S., Shimizu T., Kano R., Bando T., Ishikawa R., Giono G., Tsuneta S., Nakayama S., Tajima T., 2015, "Development of the precise polarization modulator for the Chromospheric Lyman-Alpha SpectroPolarimeter (CLASP) sounding rocket experiment", *Solar Phys.*, Accepted, DOI:10.1007/s11207-015-0774-0

Kano R., Bando T., Narukage N., Ishikawa; R., Tsuneta S., Katsukawa Y., Kubo M., Ishikawa S., Hara H., Shimizu T., Suematsu Y, Ichimoto K., Sakao T., Goto M., Kato Y., Imada S., Kobayashi K., Holloway T., Winebarger A., Cirtain J., De Pontieu B, Casini R., Trujillo Bueno J., Štěpán J., Manso Sainz R., Belluzzi L., Asensio Ramos A., Auchére F., Carlsson M., "Chromospheric Lyman-Alpha Spectro-Polarimeter (CLASP)", *Proc. SPIE*, 2012, **8443**, DOI:10.1117/12.925991

Kano R., Trujillo Bueno J., Winebarger A., Auchère F., Narukage N., Ishikawa R., Kobayashi K., Bando T., Katsukawa Y., Kubo M., Ishikawa S., Giono G., Hara H., Suematsu Y., Shimizu T., Sakao T., Tsuneta S., Ichimoto K., Goto M., Belluzzi L., Štěpán J., Asensio Ramos A. , Manso Sainz R., Cirtain J., De Pontieu B., Casini R., Carlsson M., "Discovery of Scattering Polarization in the Hydrogen Lyman-α Line of the Solar Disk Radiation", 2016, In preparation

Kobayashi K., Tsuneta S., Trujillo Bueno J., Cirtain J. W., Bando T., Kano R., Hara H., Fujimura D., Ueda K., Ishikawa R., Watanabe H., Ichimoto K., Sakao T., De Pontieu B., Carlsson M., Casini R., et al., "The Chromospheric Lyman-Alpha SpectroPolarimeter: CLASP", *Astron. Soc. Pacific*, 2012, CS-456, 233, ADS

Kubo M., Katsukawa Y., Suematsu Y., Kano R., Bando T., Narukage N., Ishikawa R., Hara H., Giono G., Tsuneta S., Ishikawa S., Shimizu T., Sakao T., Winebarger A., Kobayashi K., Cirtain J., Champey P., Auchère F., Trujillo Bueno J., Asensio Ramos A., Štěpán J., Belluzzi L., Manso Sainz R., De Pontieu B., Ichimoto K., Carlsson M., Casini R., Goto M., "Discovery of Ubiquitous Fast Propagating Intensity Disturbances by the Chromospheric Lyman Alpha Spectropolarimeter (CLASP)", *Astrophys. J.*, 2016

Landi Degl'Innocenti E., Landolfi M. , "Polarization in spectral lines.", *Astrophysics and Space Science Library*, 2004, **307**, Springer Netherlands, DOI:10.1007/1-4020-2415-0

Lemen J., Title A., Akin D., Boerner P., Chou C., Drake J., Duncan D., Edwards C., Friedlaender F., Heyman G., Hurlburt N., Katz N., Kushner G., Lindgren M., Mathur D., McFeaters E., Mitchell S., Rehse R., Schrijver C., Springer L., Stern R., Tarbell T., Wuelser J-P, Wolfson J., Yanari C., Bookbinder J., Cheimets P., Caldwell D., Deluca E., Gates R., Golub L., Park S., Podgorski W., Bush R., Scherrer P., Gummin M., Smith P., Auker G., Jerram P., Pool P., Soufli R., Windt D., Beardsley S., Clapp M., Lang J. and Waltham N., "The Atmospheric Imaging Assembly (AIA) on the Solar Dynamics Observatory (SDO)", *Solar Phys.*, 2012, **275**, 17, DOI:10.1007/s11207-011-9776-8

Narukage N., Auchére F., Ishikawa R., Kano R., Tsuneta S., Winebarger A., Kobayashi K., 2015, "Vacuum ultraviolet spectropolarimeter design for precise polarization measurements", *Applied Optics*, 2015, **54**, No.8, DOI:10.1364/AO.54.002080

Štěpán J., Trujillo Bueno J., Carlsson M., Leenaarts J., "The Hanle Effect of the Lyα in a MHD model of the Solar Transition Region", *Astrophys. J. Lett.*, 2012, **758**, DOI:10.1088/2041-8205/758/2/L43

Štěpán J., Trujillo Bueno J., Leenaarts J., Carlsson M., "Three-dimensional radiative transfer simulations of the scattering polarization of the hydrogen Lyα line in a MHD model of the chromosphere-corona transition region", *Astrophys. J.*, 2015, **803**, DOI:10.1088/0004-637X/803/2/65

Trujillo Bueno J., Štěpán J., Casini R., "The Hanle Effect of the Hydrogen Ly Line for Probing the Magnetism of the Solar Transition Region", *Astrophys. J.*, 2011, **738**, DOI:10.1088/2041-8205/738/1/L11

Trujillo Bueno J., "Polarized radiation observables for probing the magnetism of the outer solar atmosphere", *ASP Conf. Series*, 2014, **489**, 137